All-in-one trifunctional strategy: a cell adhesive, bacteriostatic and bactericidal coating for titanium implants

Mireia Hoyos-Nogués,[1,2] Judit Buxadera-Palomero,[1,2] Maria-Pau Ginebra,[1,2,3] José María Manero,[1,2] F.J Gil[1,4] and Carlos Mas-Moruno[1,2*]

[1] *Biomaterials, Biomechanics and Tissue Engineering Group (BBT), Department of Materials Science and Metallurgical Engineering, Technical University of Catalonia (UPC), 08019 Barcelona, Spain*

[2] *Barcelona Research Center in Multiscale Science and Engineering, UPC, 08019 Barcelona, Spain*

[3] *Institute for Bioengineering of Catalonia (IBEC), 08028 Barcelona, Spain*

[4] *Universitat Internacional de Catalunya (UIC), 08195 Sant Cugat del Vallès, Spain*

*Corresponding Author:
E-mail: carles.mas.moruno@upc.edu
Telephone: +34 93 401 08 14
Fax: +34 93 401 67 06

Num. Words: 5961-> 5511
Num. Figures: 6

1

Abstract

Strategies to inhibit initial bacterial adhesion are extremely important to prevent infection on biomaterial surfaces. However, the simultaneous attraction of desired eukaryotic cells remains a challenge for successful biomaterial-host tissue integration. Here we describe a method for the development of a trifunctional coating that repels contaminating bacteria, kills those that adhere, and promotes osteoblast adhesion. To this end, titanium surfaces were functionalized by electrodeposition of an antifouling polyethylene glycol (PEG) layer and subsequent binding of a peptidic platform with cell-adhesive and bactericidal properties. The physicochemical characterization of the samples via SEM, contact angle, FTIR and XPS analysis verified the successful binding of the PEG layer and the biomolecules, without altering the morphology and topography of the samples. PEG coatings inhibited protein adsorption and osteoblast-like (SaOS-2) attachment; however, the presence of cell adhesive domains rescued osteoblast adhesion, yielding higher values of cell attachment and spreading compared to controls ($p<0.05$). Finally, the antibacterial potential of the coating was measured by live/dead assays and SEM using *S. sanguinis* as a model of early colonizer in oral biofilms. The presence of PEG layers significantly reduced bacterial attachment on the surfaces ($p<0.05$). This antibacterial potential was further increased by the bactericidal peptide, yielding values of bacterial adhesion below 0.2% ($p<0.05$). The balance between the risk of infection and the optimal osteointegration of a biomaterial is often described as "the race for the surface", in which contaminating bacteria and host tissue cells compete to colonize the implant. In the present work, we have developed a multifunctional coating for a titanium surface that promotes the attachment and spreading of osteoblasts, while very efficiently inhibits bacterial colonization, thus holding promise for application in bone replacing applications.

Keywords: polyethylene glycol, antibacterial osteointegration, multifunctionality, peptides, titanium.

1.   INTRODUCTION

Biomaterial-associated infection (BAI) is a common complication that represents a major threat in modern medicine [1,2]. In fact, it has been estimated that at least 50% of all infections acquired in a hospital are implant-related [3]. Infection at an implant begins with the colonization of the surface with only a few pathogenic bacteria. In a friendly environment, even small numbers of bacteria will multiply and form a protective and resistant biofilm [4,5], which may require removal of the implant and prolonged treatment time [6]. The difficulties in the treatment of these infections arise from the fact that, once established, biofilms are very difficult to eradicate and resistant to antibacterial agents [7]. Moreover, a crucial feature of BAI is that microbial cells may detach from biofilms and disseminate to the surrounding tissues, further aggravating the clinical outcome of the infection [8]. Thus, the inhibition of bacterial adhesion is often regarded as the most critical step to prevent BAI.

Bacterial repellent coatings can be used for such purpose and to produce low fouling biomaterials that are resistant to initial bacterial attachment [9]. Among many different methods, the immobilization of polar polymers such as polyethylene glycol (PEG) [10] has been widely studied. PEG chains are highly hydrophilic and flexible [11], when immobilized on a surface form a wide exclusion volume that inhibits protein and cell adhesion [12–14].

Alternatively, bacterial colonization of biomaterials can also be inhibited by bactericidal approaches that directly kill bacteria. Examples include coatings that interact with bacterial cell membranes disrupting them or that release biocides targeting existing biofilms (i. e. antibiotics [15,16]), have been extensively studied, but the emergence of bacterial resistance towards these molecules limits their use [1,17]. For this reason, the use of antimicrobial peptides (AMPs) in biomaterials represents an option that is gaining increasing popularity [18–20]. AMPs are considered advantageous as therapeutic agents due to their broad spectrum of activity, high efficacy at low concentrations and limited tendency to develop bacterial resistance [19]. Notwithstanding the potential of AMPs, it should be emphasized that even very low numbers of surviving bacteria might proliferate and create biofilms. Furthermore, proteins from the

extracellular environment as well as secreted by dead bacteria may serve as nutrients and substrate for other bacterial colonizers [21,22].

The eradication of bacteria on the surfaces together with their related products, could be solved using biomaterials that combine both anti-adhesive (bacterial repellent) and bactericidal properties [5,22]. Such dual antibacterial function would greatly reduce initial bacterial adhesion, kill bacteria able to adhere and inhibit the accumulation of bacterial proteins and debris. In this regard, some recent examples have focused on incorporating bactericidal agents on antifouling polymers [23–26] or copolymers based on antifouling and bactericidal polymers [27,28].

However, the ideal coating would be one that not only repels and kills contaminating bacteria, but also encourages host tissue integration [29,30]. This is critical in determining the future of the implanted material, as an incomplete osteointegration may result in poor mechanical fixation and compromise the stability of the implant [31]. Designing an anti-adhesive surface that avoids bacterial infection and simultaneously shows good cell and tissue biocompatibility remains a challenge: the use of non-fouling polymers reduces the adhesion of eukaryotic cells and many bactericidal compounds compromise normal cell functions. These limitations could be solved by incorporating both cell adhesive molecules (to rescue cell adhesion) and AMPs (to replace the use of antibiotics) on polymeric antifouling substrates [32]. Nonetheless, until now, most multifunctional strategies have focused on combining cell adhesive motifs with either antifouling coatings [33,34] or bactericidal molecules [35–37]. The combination of the three approaches has rarely been explored.

Herein, we present a trifunctional coating that combines cell adhesive, bacteriostatic and bactericidal properties to functionalize biomaterials (**Fig**. 1). In detail, our all-in-one approach integrates:

i) The antifouling properties of PEG (bacteriostatic effect);

ii) the cell adhesive potential of the RGD sequence;

iii) and the antibacterial properties of the LF1-11 peptide (bactericidal effect) [38,39].

To this end, we propose a non-time consuming and straightforward method based on the electrodeposition of PEG on titanium [40–42] and subsequent immobilization of a peptidic

4

platform (PTF) previously developed by us [36], which simultaneously presents the two peptide sequences (RGD + LF1-11). The positive effects of the RGD integrin binding peptide in promoting cell adhesion on biomaterials are well established [43,44]. As AMP, the molecule selected was the LF1-11 peptide; a synthetic peptide comprising the first 11 residues at the N-terminal of the protein lactoferrin, which retains the antibacterial properties of the whole protein. LF1-11 recognizes bacteria with high sensitivity [45] and has been shown to interfere with the attachment of primary colonizers and early biofilm formation on Ti and other biomaterial surfaces [36,38].
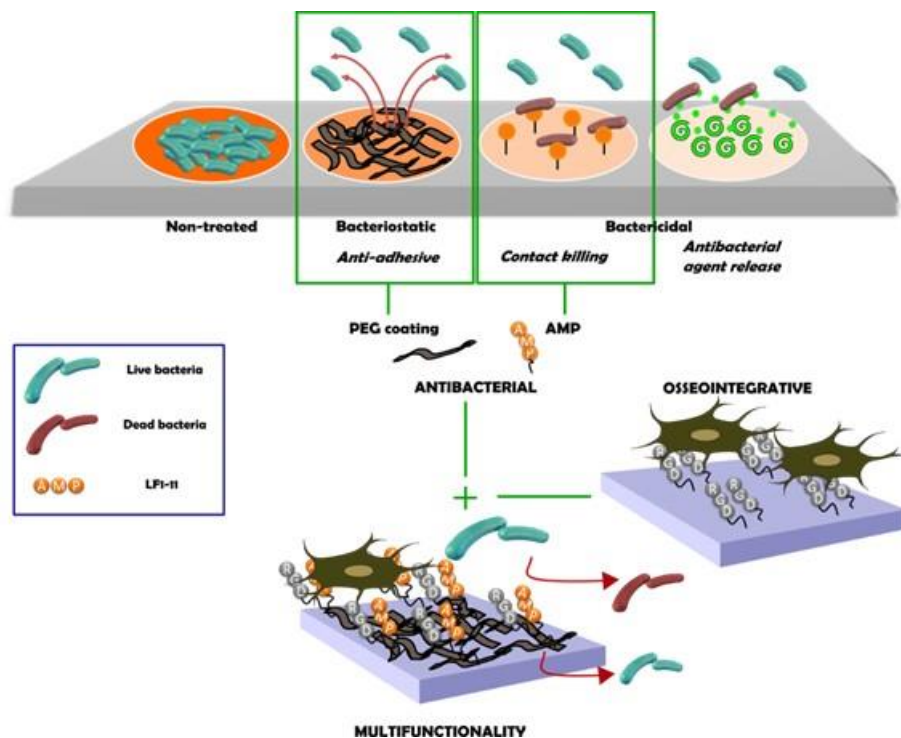

Fig. 1 Schematic representation of the trifunctional coating on the biomaterial surface. Antibacterial strategies commonly include bacteriostatic coatings, immobilized antimicrobial peptides or the release of bactericidal agents such as antibiotics or QACs. Our approach combines a PEG-based anti-adhesive coating with a multifunctional PTF that simultaneously promotes cell adhesion (RGD motif) and inhibits bacterial attachment (LF1-11 peptide).

2. MATERIALS AND METHODS

2.1. Biofunctionalization process

2.1.1. Sample preparation

Titanium (Ti) commercially pure (c.p.) grade 2 disks (10 mm diameter, 2 mm thickness) were grinded with silicon carbide papers and polished to a surface roughness (Ra) under 40 nm with suspensions of alumina particles (1 µm and 0.05 µm particle size) on cotton clothes. Once polished, samples were ultrasonically cleaned with cyclohexane, isopropanol, distilled water, ethanol and acetone (3 x 5 min each) and dried with nitrogen.

2.1.2. Coating molecules

Polyethylene glycol bis (3-aminopropyl) terminated (PEG-amine, Mn≈1500, Sigma Aldrich, USA) was used for the electrodeposition process. The platform (PTF) containing the cell adhesive (RGD) and antimicrobial peptides (LF1-11: MPA-PEG-GRRRRSVQWCA-NH$_2$; MPA = 3-mercaptopropionic acid; PEG = 2 units of 8-amino-3,6-dioxaoctanoic acid) was manually synthesized in solid-phase following the Fmoc/tBu strategy. The detailed synthetic protocol has been described elsewhere [46] and its structure characterized in previous reports [36].

2.1.3. Surface functionalization

Prior to PEG electrodeposition, Ti disks were cleaned and activated by means of low pressure plasma treatments using a 13.52MHz radiofrequency commercial reactor "Diener Femto" (Diener, Germany). For each treatment 3 samples were placed horizontally on a quartz tray in the center of the reactor and activated with argon plasma (5min, 100W) following conditions optimized in a previous study [10].

Next, a thin layer of PEG was placed to the surface by means of an electrodeposition process, which had been adapted from the technique developed by Tanaka and collaborators [40,41] and further optimized by our group in subsequent studies [47]. The system consists in a two-electrode electrolytic cell connected to a power supply that generates a continuous voltage at 5V during 5 min (see **Fig.** S1 in the Supplementary material). LABVIEW® software (National Instruments, Spain) was used to generate a square wave with periods of 8 ms, and the output signal was

controlled by an oscilloscope (DSO1052B, Agilent Technologies, Spain). The solution for the electrodeposition process was composed by 2% w/w of PEG-amine and 0.3M of NaCl, which were dissolved in 150 mL of distilled water. After electrodeposition, each sample was submerged in deionized water. To obtain the trifunctional coatings, the amine groups of the PEG layer were functionalized with the crosslinker (CL) N-succinimidyl-3-maleimidopropionate (Alfa Aesar, Germany) and the PTF was subsequently coupled at a 100 µM concentration in phosphate-buffered saline (PBS) at pH= 6.5 overnight. Uncoated polished Ti disks (Ctrol) and fibronectin-coated disks (FN) were selected as negative and positive controls for the cell adhesion assays, respectively.

2.2. Physicochemical characterization

2.2.1. Surface topography

The average surface roughness of the samples (Ra) and the roughness skewness (Rsk) were determined by white light interferometry using a Wyko NT9300 Optical Profiler (Veeco Instruments, USA) in vertical scanning interferometry mode. Three measurements were collected at different positions on three samples per group. Roughness data was analyzed with Wyko Vision 4.10 software (Veeco Instruments). The morphology of the samples was studied by means of scanning electron microscopy (SEM) (Zeiss Neon 40 FE-SEM, Carl Zeiss NTS GmbH, Germany). Images were taken for each surface at a working distance of 7 mm and a potential of 5 kV. A focused ion beam (FIB-SEM) was used to investigate the cross section and to calculate the thickness of the PEG layer obtained. The milling was carried out at beam current of 50 pA, while the energy of ions was 30 kV. Before cutting, a thin layer of protective platinum (Pt) was deposited on the surface by ion-beam-assisted deposition to reduce the curtaining effect.

2.2.2. Contact angle analysis

Contact angle using the sessile drop method was performed to measure the wettability of the samples (Contact Angle System OCA15 plus, Dataphysics, Germany). Ultrapure distilled water (volume of 3 µL) (Millipore Milli-Q, Merck Millipore Corporation, USA) was used as working fluid. Measurements were acquired in triplicate at room temperature and data was analyzed with SCA 20 software (Dataphysics).

2.2.3. Surface chemical composition

The chemical composition (atomic percentage) at the surface level was analyzed by X-ray photoelectron spectroscopy (XPS). XPS spectra of the samples were acquired with a non-monochromatic Mg anode X50 source, operating at 150 W and a Phoibos 150 MCD-9 detector (D8 advance, SPECS Surface Nano Analysis GmbH, Germany). Detector pass energy was fixed at 25 eV with 0.1 eV steps to record high resolution spectra at a pressure below 7.5×10^{-9} mbar. Peak fittings and spectral analysis were conducted using Casa XPS software (Version 2.3.16, Casa Software Ltd., UK) and all binding energies were referenced to the C1s signal (284.8 eV). Three samples of each condition were studied.

Fourier Transformed Infrared Spectra were recorded using a FTIR Nicolet 6700 in the Attenuate Total Reflectance mode (ATR-FTIR) (256 scans with a $2cm^{-1}$ data spacing resolution). ATR-FTIR was used to control the presence of PEG and PTF in the biofunctionalized samples.

2.3. Biological characterization

2.3.1. Protein Adsorption

Ti samples were immersed in bovine serum albumin (BSA, Sigma Aldrich, USA) stained with Fluorescein Isothiocyanate (FITC) solution. Pierce Antibody Labeling Kit (Thermo Scientific, USA) was used to label the protein, according to manufacturer's instructions. Briefly, BSA was dissolved in a phosphate-borate buffer, mixed with FITC and purified in a spin column with purified resin to remove the non-reacted FITC.

Samples were then immersed in 100 µL of FITC-BSA at a concentration of 100 µg/mL during 1 h in the dark. After fixing with paraformaldehyde (PFA, Sigma Aldrich, USA), samples were washed with PBS. Finally, samples were examined under a Nikon E-600 fluorescence microscope (Nikon Corporation Instruments Company, USA). To quantify protein adsorption, five images were taken for each sample and the Fiji/Image-J package (NIH, MD, USA) was used to calculate pixel intensity.

2.3.2. Cell culture

Mc Coy's 5A medium was supplemented with 10% (v/v) fetal bovine serum (FBS), 2% (v/v) 4-(2-hydroxyethyl)-1-piperazineethanesulfonic acid (HEPES), 1% (w/v) sodium pyruvate, 50 µg/mL streptomycin, 50 U/mL penicillin and 1% (w/v) L-glutamine. Human sarcoma osteogenic (SaOS-2) cells (ATCC, USA) were maintained in culture medium at 37ºC in a humidified atmosphere containing 5% (v/v) CO_2 and culture medium was changed twice a week. Confluent cells were detached by trypsin-EDTA and subcultured into a new flask. The experiments were carried out with cells at passages 25-35. All reagents were purchased from Sigma–Aldrich, unless otherwise noted.

2.3.3. Cell adhesion

The number of adherent cells on Ti surfaces was obtained by the quantification of the enzymatic activity of lactate dehydrogenase (LDH) by means of a conventional colorimetric assay (Cytotoxicity Detection Kit (LDH), Roche Diagnostics, Germany). After the functionalization process, samples were rinsed three times with PBS and SaOS-2 cells were seeded at 5×10^4 cells/mL (25.000 cells per disk) in serum free medium and incubated at 37 ºC for 4 h. After this time, samples were rinsed with PBS to remove non-adherent cells, and remaining cells were lysed with 350 µL/disk of mammalian protein extraction reagent (M-PER). LDH activity was quantified by absorbance measurements using a multimode microplate reader (Infinite M200 PRO, Tecan Group Ltd., Switzerland). A standard curve of defined cell concentrations was defined to obtain cell numbers from the absorbance read-out of the test. Cells seeded in the TCPS were used as the positive control, and culture media as the negative control.

2.3.4. Immunofluorescence analysis

For cell morphology inspection, an immunofluorescence analysis of the biofunctionalized samples was performed. To this end, after 4 h in serum-free medium incubation, cells were fixed 20 min with PFA (4% w/v in PBS), permeabilized 20 min with 0.05% (w/v) Triton X-100 in PBS and blocked 30 min with 1% BSA (w/v) in PBS. Actin fibers were stained 1 h by incubating with TRITC-conjugated phalloidin (1:300, in permeabilizing buffer) and nuclei were stained 2 min using 4',6-diamidino-2-phenylindole (DAPI) (1:1000, in PBS-glycine 20 mM), both in the dark.

Between all steps, samples were rinsed three times with PBS-glycine for 5 min. Ti disks were mounted and visualized under a fluorescence inverted microscope (AF7000, Leica, Germany) and images processed using Fiji/Image-J package to calculate number of cells and their spreading.

2.3.5. Bacterial culture

Bacterial adhesion assays were done using *S. sanguinis* as bacterial strain. *S. sanguinis* was chosen as a model of primary colonizer in biofilm formation and was obtained from Colección Española de Cultivos Tipo (CECT 480, Spain). Bacteria were grown overnight at 37 ºC in Todd-Hewitt (TH) broth (Scharlab SL, Spain). The optical density of each bacterial suspension was measured at 600 nm (OD600) and adjusted to around 0.2, corresponding to a bacterial concentration of 10^8 colony forming unit (CFU)/mL. The assays were performed in static conditions and using three replicates for each condition.

2.3.6. Bacterial viability and adhesion at early stages of biofilm formation

After sterilization with ultraviolet (UV) irradiation for 10 min and washing twice with PBS, functionalized samples were transferred to a 48-well plate and incubated with 40 µL of *S. sanguinis* at 1×10^8 CFU/mL during 4 h at 37 ºC.

The viability of bacteria was measured using a LIVE/DEAD BackLight Bacterial Viability Kit (ThermoFisher, Spain). Dead bacterial cells were stained with the red-fluorescent nucleic acid staining agent propidium iodide, which only penetrates damaged cell membrane, while all bacterial cells were labeled with SYTO 9 green-fluorescent nucleic acid staining agent, which can penetrate cells both with intact and damaged membranes. With an appropriate mixture of the SYTO 9 and propidium iodide stains, bacteria with intact cell membranes stain fluorescent green, whereas bacteria with damaged membranes stain fluorescent red. After incubation time (4 h), the samples were washed three times with PBS and 100 μL of a solution containing the two dyes was added on the surface. The solution containing the dyes was prepared by mixing 3 μL of SYTO and 3 μL of propidium iodide in 2 mL of PBS buffer. The samples were incubated at room temperature in the dark for 15 min and the attached bacteria were visualized using a Zeiss LSM 800 confocal microscope (Carl Zeiss, Jena, Germany). The confocal LIVE/DEAD images were

acquired using Zen 2.3 software (Carl Zeiss), the specimens were observed with a 10x lens. The area covered by bacteria was analyzed and quantified using ImageJ software. The volume ratio of red fluorescence (dead cells) versus green (live cells) indicated the portion of killed cells for each treatment:

$$volume\ ratio\ of\ dead\ cells = red\ bacteria\ /\ green\ bacteria$$

Bacterial attachment and morphology on Ti surfaces were further analyzed by SEM. To this purpose, bacteria were fixed with 3% (v/v) glutaraldehyde in phosphate buffer 0.1 M for 50 min. Prior to SEM analysis, samples were dehydrated in graded alcohol (ranging from 30% to 100% (v/v)) and sputter coated with carbon (Sputter Coater SCD005, BAL-TEC, Liechtenstein). To compare with antibacterial results obtained in a previous work, where the PTF was covalently attached to the Ti [36], surface functionalization of this additional condition was accomplished by means of a three-step procedure: (1) silanization with APTES in anhydrous toluene; (2) cross-linking with CL in DMF; and (3) PTF immobilization in PBS. This protocol has been carefully described in previous studies [48,49].

2.4.   Statistical analysis

Statistically significant differences between groups were assessed by parametric 1-way ANOVA test followed by post hoc pairwise comparisons using Tamhanne and Scheffe post hoc test depending on the homogeneity of the variance. Differences were also analyzed by non-parametric Kruksall-Wallis test. Values of all graphs are reported as mean ± standard deviation. The software used for statistical analysis was SPSS statistics (IBM, USA).

3.   RESULTS

3.1.   Physicochemical characterization of biofunctionalization process

Values for roughness, arithmetic average height (Ra) and the surface skewness (Rsk), are shown in **Table S1** (see Supplementary material). A statistically significant decrease in surface roughness was observed after the polishing process, yielding negative values of Rsk. The electrodeposition of PEG on polished samples did not result in significant differences in surface roughness values.

Scanning electron microscopy (SEM) was used to further study the morphology of Ti surfaces after PEG electrodeposition. As shown in **Fig.** S2 A (Supplementary material), Ctrol Ti samples displayed a homogeneous smooth surface. This texture was not affected by the electrodeposition of PEG molecules on the surfaces. A high-resolution cross-sectional FIB-SEM image of the PEG coatings is presented in **Fig.** S2 B (Supplementary material) and image analysis determined the thickness of PEG layer was of 25±5 nm.

The sessile drop method was used to measure the contact angle of the entire functionalization process (**Fig.** 2 A). Plasma treatment renders a higher surface hydrophilicity, compared to Ctrol samples. In contrast, the subsequent addition of the PEG coating, the cross-linker (CL) and the bioactive molecule (PTF) significantly increased the water contact angle. However, all conditions rendered contact angle values lower (less hydrophilic) than Ti Ctrol.
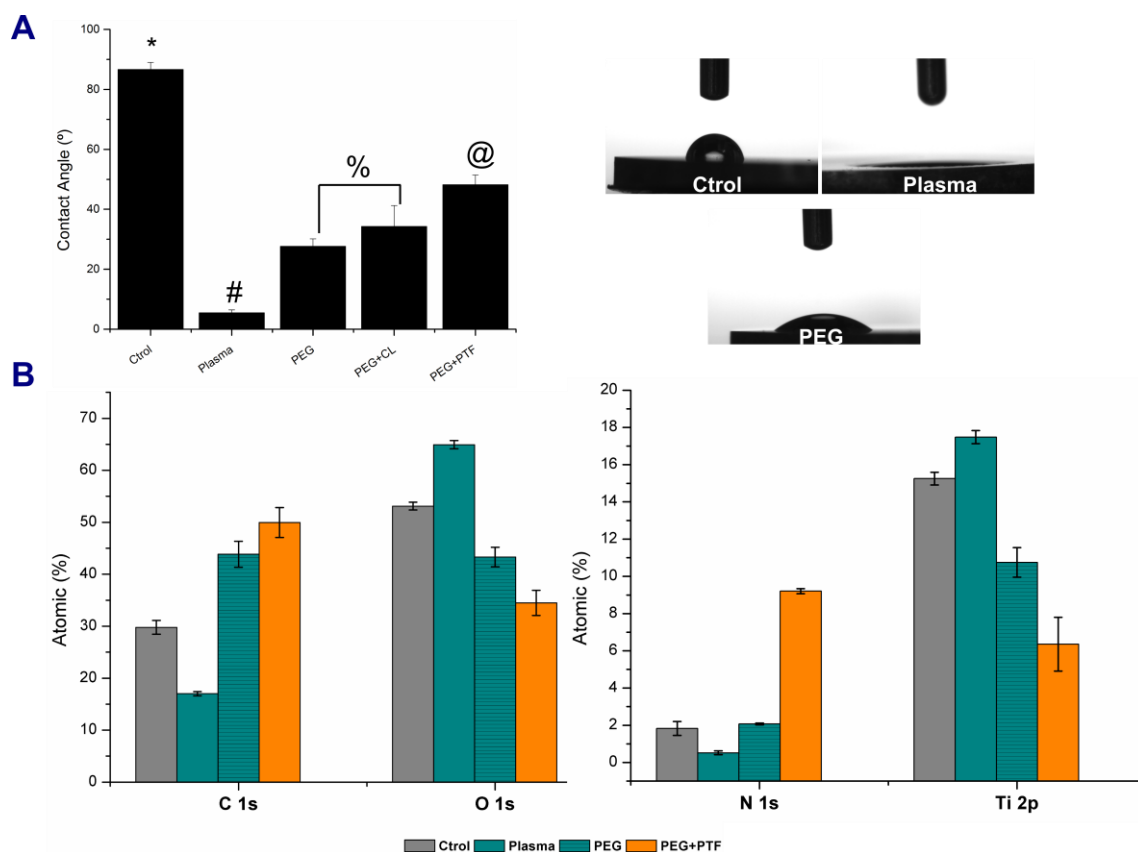
Fig. 2 (A) Water contact angle of the different steps of the biofunctionalization process. Samples with the same symbol have no statistically significant differences (p<0.05). Images of water droplet contact angle measurements. **(B)** Surface chemical composition (atomic percentages) of the functionalization process by XPS. All conditions are statistically different compared to the previous step of the protocol (p < 0.05).

The presence of the PEG layer was also confirmed by XPS (**Fig.** 2 B). XPS analysis of plasma-activated samples showed a decrease in the carbon amount compared to untreated Ti (Ctrol), which was accompanied with an increase in Ti and oxygen signals. In contrast, the deposition of a PEG coating followed an opposite trend with an increase in the C1s and N1s signals and a reduced detection of the Ti levels. Both effects can be easily correlated to the presence of PEG-amine molecules. The immobilization of the platform on the PEG layer resulted in further changes in the chemical composition of the samples: the percentages of C 1s and N 1s augmented, while the O 1s and Ti 2p signals were reduced.

ATR-FTIR was further used to characterize the presence of the PEG and the attachment of the PTF (**Fig.** 3 A). ATR-FTIR spectra displayed distinctive peaks of both the PEG coating and the presence of the PTF on the surfaces. These characteristic signals are numbered in **Fig.** 3 and can

be correlated to their respective vibrational modes. For instance, the band between 3560 and 3760 cm^{-1} can be assigned to the skeletal vibration of the O−H bond stretching of PEG chains (**Fig.** 3 A, band 1). The range of wavelength numbers between 1330-1450 cm^{-1} was attributed to CH scissoring and bending of the PEG and PTF molecules (**Fig.** 3 B and **Fig.** 3 C, band 2). The vibrational bands between 1000-1260 cm^{-1} were assigned to C−O and C−O−C bonds (**Fig.** 3 B, band 3). In particular, the signal at 1108 cm^{-1} was attributed to C−O stretching, characteristic of the ether bonds of PEG (**Fig.** 3 B, band 4). With the addition of the PTF, new bands were observed between 1100-1300 cm^{-1}, corresponding to amide bonds of the biomolecules (C−N stretching, **Fig.** 3 C, widening of band 3). Also, stronger transmittance for C−O and C−O−C bonds **Fig.** 3 C, bands 3 and 4) was observed when the PTF was added to the surface.
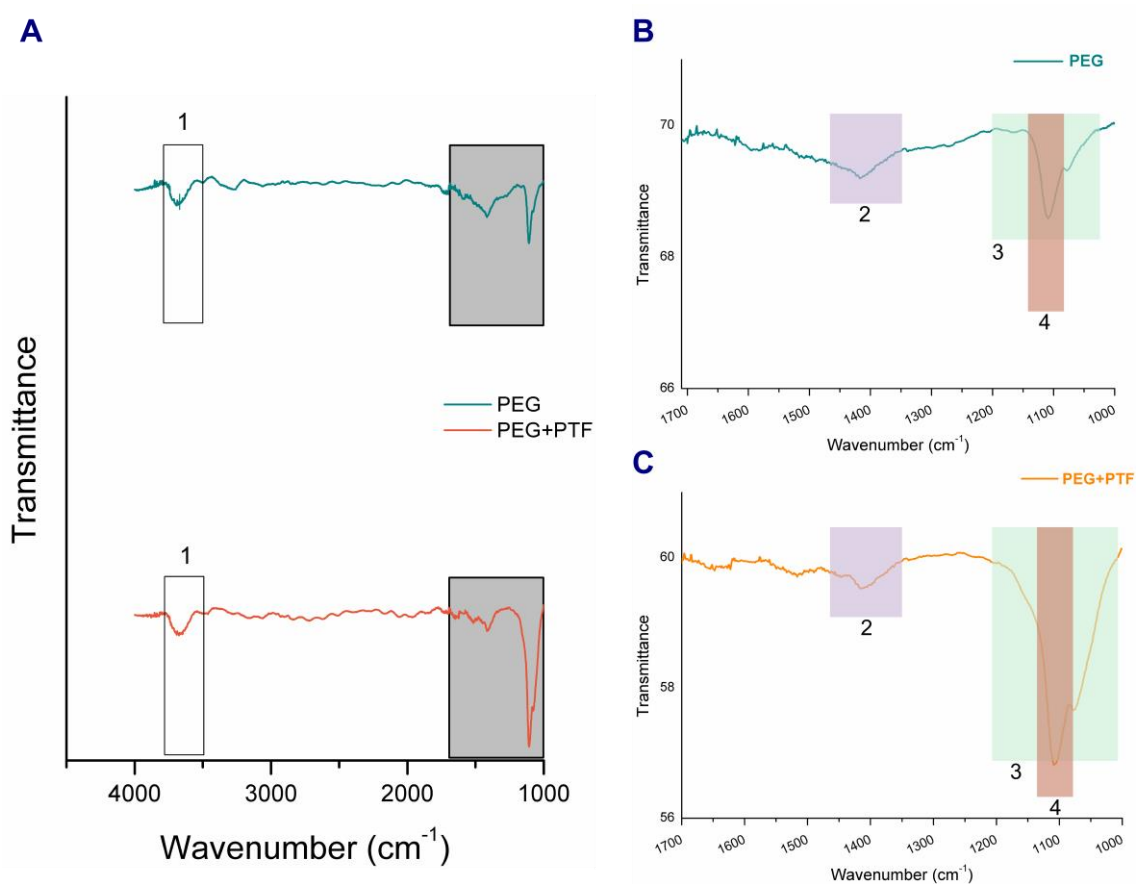

Fig. 3 (A) ATR-FTIR of PEG and PEG+PTF conditions. (B) Zoom (1700-1000 cm^{-1}) for PEG. (C) Zoom (1700-1000 cm^{-1}) for PEG+PTF.

3.2.   Protein adsorption

As shown in **Fig. S3** A (see Supplementary material), albumin adsorption on Ti samples was significantly reduced after PEG electrodeposition, yielding surfaces with very low values of protein adsorption. The presence of the PTF biomolecule did not modify these values. Fluorescent microscopy images on **Fig. S3** B display a very homogeneous protein coverage on Ctrol Ti samples, which is greatly inhibited when the PEG layers are present.

3.3.   Osteoblast-like behavior on biofunctionalized surfaces

The adhesion of SaOS-2 cells onto the different substrates was investigated by LDH analysis and immunofluorescence techniques to understand the influence of surface biofunctionalization on cell behavior (**Fig. 4**). Cell adhesion was affected by the presence of the PEG-coating; which supported the lowest numbers of cell attachment and spreading. Noteworthy, cells completely failed to spread on PEG surfaces, adopting a highly rounded morphology **Fig. 4** C, **4** D). This correlates with an almost absence of LDH signal (**Fig. 4** A). In contrast, the PTF (PEG+PTF) satisfactorily rescued cell adhesion, yielding a statistically significant increase in both cell attachment and area in comparison to Ctrol and PEG conditions. These values were lower to those observed in FN-coated samples, used as positive control, which exhibited the highest values of cell adhesion.
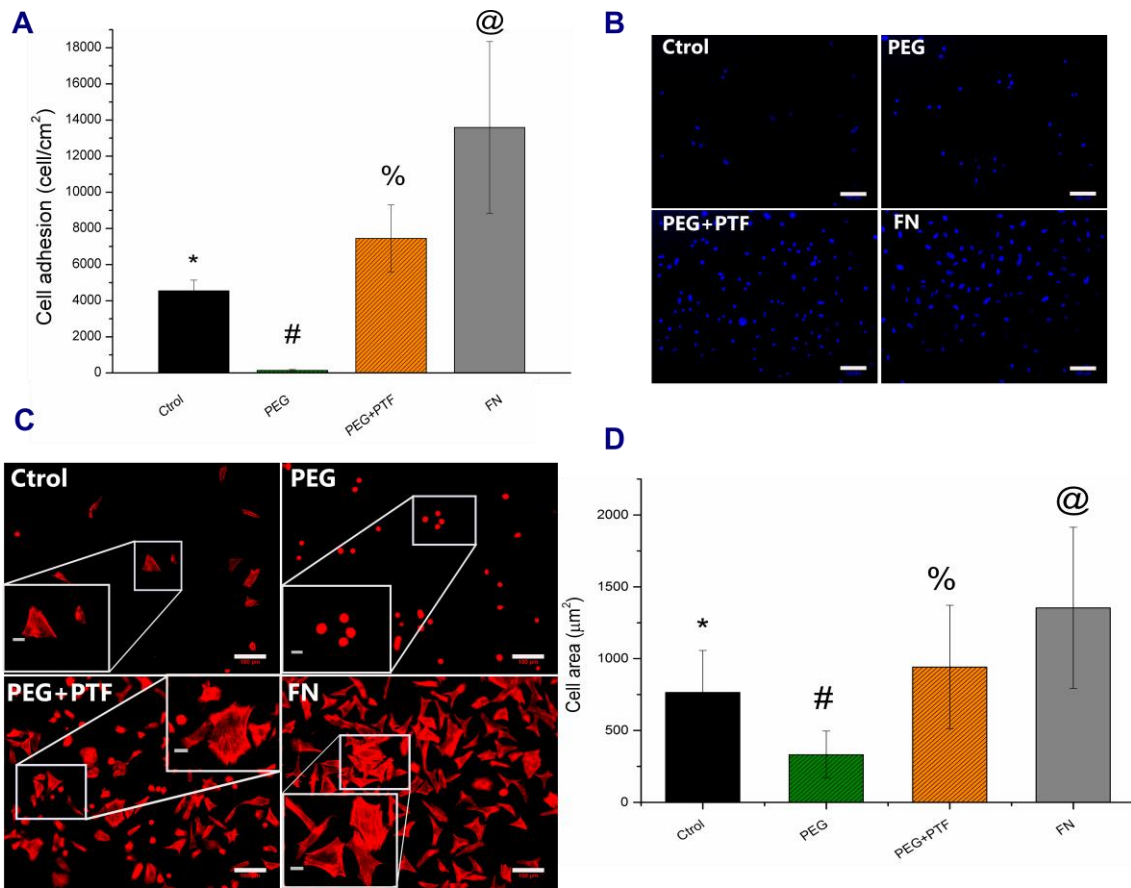
Fig. 4 (A) Cell attachment (cells/cm^2) after 4 h of incubation in serum-free medium. Cell number was quantified by LDH measurement. (B) Fluorescent staining of nuclei (scale bar = 100 μm) after 4 h of incubation in serum-free medium. (C) F-actin immunostaining (scale bar = 100 μm, scale bar = 20 μm in the insets). (D) Projected cell area (μm^2). Symbols (*, #, %, @) indicate statistically significant differences between conditions with p < 0.05.

3.4.   Antibacterial properties of the biofunctionalized surfaces

The attachment and viability of *S. sanguinis* on the biofunctionalized samples was tested using a live/dead staining after 4 h of incubation (**Fig. 5**). **Fig. 5** A illustrates a homogenous coverage of *S. sanguinis* was observed on Ctrol samples. In contrast, almost no bacterial attachment was detected on the biofunctionalized samples (PEG and PEG+PTF). The percentage of bacterial adhesion was calculated as a function of surface coverage by the bacteria, and further corroborates the antibacterial potential of the treatments (**Fig. 5** B). Untreated surfaces, where a high bacterial colonization was observed, were used to define the maximum values of bacterial attachment (100%). In comparison, the area covered by bacteria and therefore the extent of bacterial adhesion was drastically reduced on PEG-coated and PEG+PTF samples ($p < 0.05$). Interestingly, the PTF statistically increased the antibacterial properties of the PEG layer (1.2% vs. 0.2% of adhesion, for PEG and PEG+PTF, respectively). The ratio of dead bacteria was also calculated and is shown in **Fig. 5** B. While the majority of bacteria were alive on Ctrol samples, the percentage of dead bacteria was increased up to 8.6% on PEG samples and 10.4% on PEG+PTF samples.

The effect of the coatings on the attachment and morphology of bacteria was further investigated by SEM (**Fig. 6**) and was compared to the covalent attachment of the PTF on Ti samples, as studied in a previous work [36]. On PEG-coated samples, the number of bacteria was significantly reduced compared to Ti samples. This decrease was more pronounced with the presence of the PTF (this was observed for both techniques of immobilization, PEG+PTF and PTF). Moreover, the PTF directly affected the morphology of *S. sanguinis*, disrupting their membranes, in comparison with Ctrol and PEG surfaces where the integrity of bacteria was not significantly altered. SEM analysis also revealed that on Ctrol and PTF conditions bacteria seemed to interact with the substrates via well-defined filaments (**Fig. 6** B, black arrows). These filamentous structures were, however, not noticed on PEGylated samples (PEG and PEG+PTF).

A

Ctrl | PEG | PEG+PTF
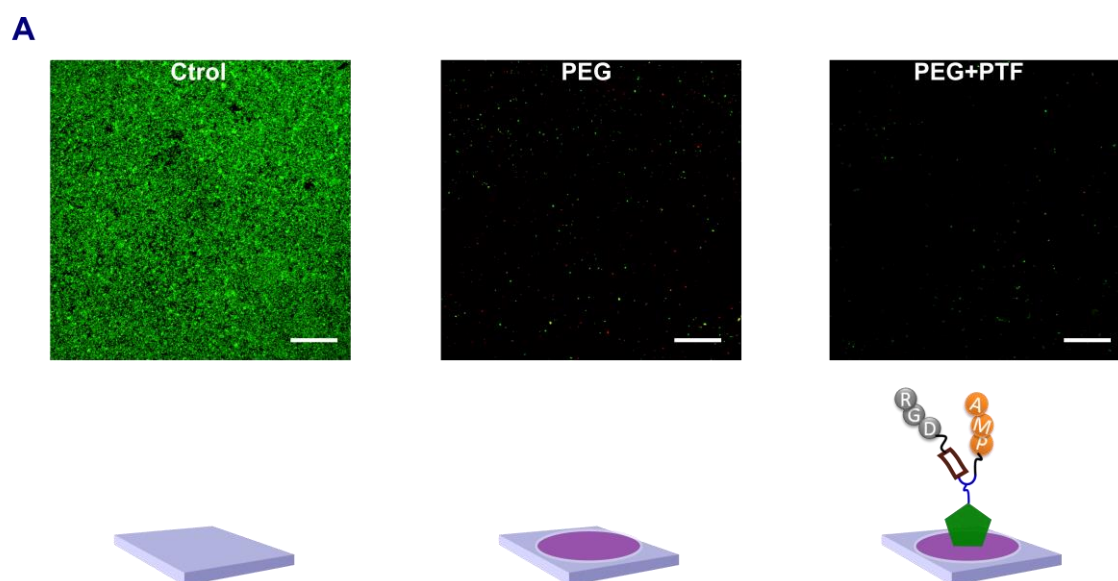
B

	Bacterial adhesion compared to Ti (%)	Ratio of dead bacteria (%)
Ctrol	100	0.4
PEG	1.2 *	8.6
PEG+PTF	0.2 #	10.4

Fig. 5 Live/dead staining of *S. sanguinis* after 4 h of incubation (A) Fluorescence microscopy images of *S. sanguinis* (scale bars = 100 μm) in Ctrol and biofuncionalized samples (PEG and PEG+PTF conditions). (B) Percentage of bacterial adhesion compared to uncoated Ti and ratio of dead bacteria for all conditions. Symbols (*, #) indicates statistically differences between conditions with p < 0.05.
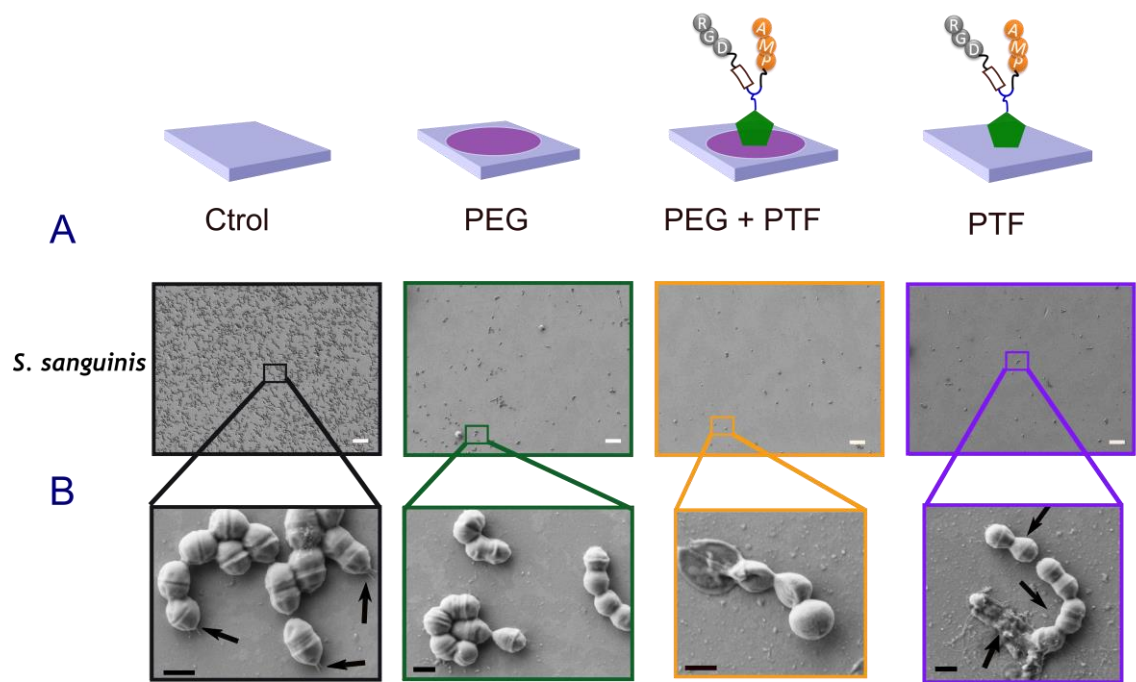
Fig. 6 (A) Bacterial adhesion on the samples for *S. sanguinis* visualized by SEM (scale bar 10 µm). (B) Magnification of SEM images to show bacterial morphology and their interaction with the surface. Black arrows indicate fimbria filaments used by bacteria to attach to the surface (scale bar 400 nm).

4. DISCUSSION

4.1. Physicochemical characterization of biofunctionalization process

The effects of the biofunctionalization treatments in the roughness and chemistry of the Ti surfaces were studied prior to the biological assays, as both properties play a major role in the biological events that follow implantation [50]. For example, surfaces roughness is known to have a strong influence in the adhesion and behavior of both bacteria and osteoblasts [51]. Thus, to exclude the influence of topographical features, samples were polished until achieving homogeneous smooth surfaces with Ra values below 40 nm (see Table S1 in Supplementary material). Ra values below 0.2 µm are considered too low to significantly affect the attachment of bacteria [52] or to promote osteoblast adhesion [53]. The roughness of the samples, once reduced by the polishing process, was not increased by the electrodeposition of PEG. On the contrary, PEGylation of the surfaces seemed to result in smoother profiles, which may be due to the filling of scratches and other irregularities of the Ti surfaces. In previous studies, we demonstrated that the presence of the PTF does not alter further the roughness of the surface [36,46,48]. Surface analysis by SEM confirmed that the texture of the samples remained unaffected through the electrodeposition process (see **Fig.** S2 A in Supplementary material) and was useful to verify the presence of a thin layer of PEG on Ti (see **Fig.** S2 B in Supplementary material), as observed in other studies [47]. In addition to surface topography, changes in wettability and surface chemistry were also examined (**Fig. 2** and **Fig. 3**). Activation of Ti by means of oxygen plasma treatment enhanced its wettability due to the combined effect of the removal of hydrophobic contaminants [54] and the formation of hydroxyl species, thus producing a more reactive surface [55]. These results were confirmed by the reduced amount of carbon and the increased percentage of O 1s and Ti 2p found by XPS. The subsequent steps of functionalization (PEG electrodeposition and PTF immobilization) were monitored by changes in water contact angles, which were in agreement with the hydrophilicity of the molecules deposited on the surfaces, and corroborated by XPS and FTIR analysis [10,56,57]. For instance, the attachment of both the PEG layer and the PTF increased C 1s and N 1s percentages, but

reduced the amount of measurable Ti 2p due to the attenuation of the substrate signal by the coating [36,46,49].

4.2. Protein adsorption

Bacterial surface adhesion molecules, which include proteins such as lectins, as well as surface carbohydrates, play a major role in bacteria-to-surface and bacteria-to-bacteria interactions [58]. Hence, creating an antifouling environment that does not facilitate protein adhesion is expected to block bacterial interactions with the surface and their eventual adhesion. To this end, a protein adsorption assay, using albumin as model protein, was performed (**Fig. S3**). Measurement of the fluorescence intensity of FITC labeled proteins is a well-established method for the determination of protein adsorption on different substrates, as the fluorescence intensity can be considered proportional to the presence of protein [59]. On the untreated polished Ti disks (Ctrol), the highest fluorescence intensity was observed, indicating Ti supports good levels of protein adsorption [60]. In contrast, the PEG coatings drastically reduce the amount of protein attachment, in agreement with their well-known antifouling properties [10,42]**.** It is important to highlight that the low fouling behavior of PEGylated surfaces was maintained after the PTF immobilization, thus indicating that neither the RGD sequence, nor the LF1-11 peptide promote any non-specific protein attachment.

4.3. Cellular and bacterial behavior on the multifunctional surfaces

It has been reported that hydrophilic and antifouling surfaces, such as PEG-coated substrates, not only avoid bacterial adherence but also inhibit mammalian cell adhesion [61]. For this reason, the use of PEGylated surfaces for preventing bacterial adherence requires further modification to rescue optimal levels of osteoblast adhesion. To this end, using cell adhesive proteins is generally not recommended, as many gram-negative and gram-positive bacteria also bind to extracellular matrix proteins like fibronectin and fibrinogen [62]. The RGD motif is known to interact specifically with cell surface integrin receptors [63], but is not recognized by bacteria, and can improve the bioactivity of the implant [36,46,64]. Hence, incorporating this peptide into low fouling PEG coatings is regarded as a viable way to enhance osteoblast functions but not bacterial adhesion [33,61]. This was clearly confirmed in our cell adhesion assays (**Fig. 4**). PEG-coating

yielded the lowest values of cell adhesion. In particular, osteoblasts failed to spread and showed highly rounded morphologies, due to the lack of integrin binding motifs on the surface (**Fig. 4** C). The fact that LDH activity was not detected on PEG surfaces (**Fig. 4** A), presumably indicates that osteoblasts observed by immunofluorescence on these substrates (**Fig. 4** B, C) were dead or in a pre-apoptotic stage. The presence of the PTF yielded a significant increase in both cell attachment, spreading and cytoskeletal formation, satisfactorily rescuing and improving the cell-adhesive capacity of the surfaces. This effect is attributed to the RGD sequence present in the peptidic PTF [36].

Having demonstrated that the multifunctional coating reduces protein adsorption but promotes osteoblast adhesion, we focused further on the antibacterial properties of the coating. It is nowadays recognized that bacterial adhesion and tissue integration are competitive processes, i.e. the "race for the surface" [65] and that early bacterial colonization is detrimental for eukaryotic cell adhesion [36]. In dental implants, biofilm formation is initiated by the adhesion of a number of early colonizers, such as *S. sanguinis* [4]. Thus, inhibiting their adhesion is crucial to avoid the development of a biofilm. Therefore, *S. sanguinis* was chosen as a model for the antibacterial assays [36,39,45].

The adhesion of *S. sanguinis* to the modified surfaces was evaluated using fluorescence and electron microscopy (**Fig. 5** and **Fig. 6**). As expected, the anti-adhesive properties of the PEG-coating resulted in a potent antibacterial (bacteriostatic) effect, significantly reducing the numbers of bacteria attached in comparison to control Ti. These observations respond to the low fouling properties of PEG, which prevent bacterial attachment as previously described by several authors [42,66]. Noteworthy, the immobilization of the PTF on PEG substrates further increased the antibacterial potential of the surfaces, reducing the extent of bacterial adhesion to very low numbers (**Fig. 5** B). Given that in previous studies we demonstrated the bactericidal properties of the LF1-11 peptide [36,67], a higher ratio of dead bacteria was expected for the PEG+PTF condition. However, dead bacteria may be washed very easily off the samples due the low adherence of the PEGylated substrates. Indeed, the bactericidal potential of LF1-11 was evident by SEM analysis (**Fig. 6**). The PTF not only reduced the number of adherent bacteria compared

to PEG alone, it also disrupted bacterial morphology. In this regard, on surfaces coated with the PTF debris consistent with bacterial fragments or dead bacteria were detected. These findings are good indicators of the direct bactericidal effect exhibited by the anchored molecules [68], well in accordance with our previous findings [36]. Another interesting aspect observed by SEM was that on Ctrol surfaces bacteria produced fine filaments that were used to bind to the surface (**Fig. 6** B, black arrows). These filamentous appendages (called fimbria) can support bacterial adhesion to solid surfaces and are involved in biofilm formation [12,69]. In contrast, on PEGylated samples (PEG and PEG + PTF) these filaments were not visible, indicating that the antifouling coating also inhibits the formation of fimbria, which are necessary for the colonization in the infection process. Taken these results together, the antibacterial properties of our coating strategy seem to arise from both the antifouling character of PEG and the bactericidal properties of the AMP. Such combined effect drastically inhibited the initial adhesion of *S. sanguinis*, and thus represent a promising approach to reduce the capacity of bacteria to develop resistant biofilms on Ti.

5.   CONCLUSIONS

To conclude, a trifunctional coating was successfully prepared by means of an easy and effective biofunctionalization method. To endow Ti surfaces with cell adhesive and antibacterial properties, the samples were coated with an antifouling PEG layer by electrodeposition, followed by the immobilization of a dual-function platform containing the RGD and LF1-11 peptides. These biofunctionalized surfaces presented a threefold activity: (i) antifouling properties to block protein adsorption and bacterial attachment (PEG); (ii) bactericidal potential to directly kill bacteria (LF1-11); and (iii) cell binding activity to enhance osteoblast growth (RGD). Thus, the strategy proposed effectively inhibited the initial adhesion of *S. sanguinis*, a primary colonizer involved in oral biofilms, and simultaneously displayed very good levels of osteoblast adhesion on Ti surfaces. Such approach holds potential for biomedical applications e.g. in dentistry, as it simultaneously addresses two major reasons of implant failure: bacterial infection and biofilm progression, and poor material osteointegration.

Appendix A. Supplementary data.
Supplementary data associated with this article can be found, in the online version, at …..

REFERENCES

1. Busscher, H. J.; van der Mei, H. C.; Subbiahdoss, G.; Jutte, P. C.; van den Dungen, J. J. a. M.; Zaat, S. a. J.; Schultz, M. J.; Grainger, D. W. Biomaterial-Associated Infection: Locating the Finish Line in the Race for the Surface. *Sci. Transl. Med.* **2012**, *4*, 153rv10-153rv10, doi:10.1126/scitranslmed.3004528.

2. Veerachamy, S.; Yarlagadda, T.; Manivasagam, G.; Yarlagadda, P. K. Bacterial adherence and biofilm formation on medical implants: A review. *Proc. Inst. Mech. Eng. Part H J. Eng. Med.* **2014**, *228*, 1083–1099, doi:10.1177/0954411914556137.

3. Chitnis, A. S.; Edwards, J. R.; Ricks, P. M.; Sievert, D. M.; Fridkin, S. K.; Gould, C. V Device-Associated Infection Rates, Device Utilization, and Antimicrobial Resistance in Long-Term Acute Care Hospitals Reporting to the National Healthcare Safely Network, 2010. *Infect. Control Hosp. Epidemiol.* **2012**, *33*, 993–1000, doi:10.1086/667745.

4. Kolenbrander, P. E.; Palmer, R. J.; Periasamy, S.; Jakubovics, N. S. Oral multispecies biofilm development and the key role of cell-cell distance. *Nat. Rev. Microbiol.* **2010**, *8*, 471–80, doi:10.1038/nrmicro2381.

5. Arciola, C. R.; Campoccia, D.; Speziale, P.; Montanaro, L.; Costerton, J. W. Biofilm formation in Staphylococcus implant infections. A review of molecular mechanisms and implications for biofilm-resistant materials. *Biomaterials* **2012**, *33*, 5967–5982, doi:10.1016/j.biomaterials.2012.05.031.

6. Norowski, P. A.; Bumgardner, J. D. Biomaterial and antibiotic strategies for peri-implantitis. *J. Biomed. Mater. Res. - Part B Appl. Biomater.* **2009**, *88*, 530–543, doi:10.1002/jbm.b.31152.

7. Holmes, A. H.; Moore, L. S. P.; Sundsfjord, A.; Steinbakk, M.; Regmi, S.; Karkey, A.; Guerin, P. J.; Piddock, L. J. V Understanding the mechanisms and drivers of antimicrobial resistance. *Lancet* **2016**, *387*, 176–187, doi:10.1016/S0140-6736(15)00473-0.

8. Costerton, W.; Veeh, R. The application of biofilm science to the study and control of chronic bacterial infections. *J. Clin. Invest.* **2003**, *112*, 12, doi:10.1172/JCI200320365.Introduction.

9. Banerjee, I.; Pangule, R. C.; Kane, R. S. Antifouling Coatings: Recent Developments in the Design of Surfaces That Prevent Fouling by Proteins, Bacteria, and Marine Organisms. *Adv. Mater.* **2011**, *23*, 690–718, doi:10.1002/adma.201001215.

10. Buxadera-Palomero, J.; Canal, C.; Torrent-Camarero, S.; Garrido, B.; Javier Gil, F.; Rodríguez, D. Antifouling coatings for dental implants: Polyethylene glycol-like coatings on titanium by plasma polymerization. *Biointerphases* **2015**, *10*, 29505, doi:10.1116/1.4913376.

11. Glinel, K.; Thebault, P.; Humblot, V.; Pradier, C. M.; Jouenne, T. Antibacterial surfaces developed from bio-inspired approaches. *Acta Biomater.* **2012**, *8*, 1670–1684, doi:10.1016/j.actbio.2012.01.011.

12. Neoh, K. G.; Kang, E. T. Combating bacterial colonization on metals via polymer coatings: Relevance to marine and medical applications. *ACS Appl. Mater. Interfaces* **2011**, *3*, 2808–2819, doi:10.1021/am200646t.

13. Gour, N.; Ngo, K. X.; Vebert-Nardin, C. Anti-infectious surfaces achieved by polymer modification. *Macromol. Mater. Eng.* **2014**, *299*, 648–668, doi:10.1002/mame.201300285.

14. Tanaka, Y.; Matsuo, Y.; Komiya, T.; Tsutsumi, Y.; Doi, H.; Yoneyama, T.; Hanawa, T. Characterization of the spatial immobilization manner of poly(ethylene glycol) to a titanium surface with immersion and electrodeposition and its effects on platelet adhesion. *J. Biomed. Mater. Res. - Part A* **2010**, *92*, 350–358, doi:10.1002/jbm.a.32375.

15. Hickok, N. J.; Shapiro, I. M. Immobilized antibiotics to prevent orthopaedic implant infections. *Adv. Drug Deliv. Rev.* **2012**, *64*, 1165–1176, doi:10.1016/j.addr.2012.03.015.

16. Rocas, P.; Hoyos-Nogues, M.; Rocas, J.; Manero, J. M.; Gil, J.; Albericio, F.; Mas-Moruno, C. Installing Multifunctionality on Titanium with RGD-Decorated Polyurethane-Polyurea Roxithromycin Loaded Nanoparticles: Toward New Osseointegrative Therapies. *Adv. Healthc. Mater.* **2015**, *4*, 1956–1960,

doi:10.1002/adhm.201500245.

17. Buffet-Bataillon, S.; Tattevin, P.; Bonnaure-Mallet, M.; Jolivet-Gougeon, A. Emergence of resistance to antibacterial agents: The role of quaternary ammonium compounds - A critical review. *Int. J. Antimicrob. Agents* **2012**, *39*, 381–389, doi:10.1016/j.ijantimicag.2012.01.011.

18. Ageitos, J. M.; Sánchez-Pérez, A.; Calo-Mata, P.; Villa, T. G. Antimicrobial peptides (AMPs): Ancient compounds that represent novel weapons in the fight against bacteria. *Biochem. Pharmacol.* **2017**, *133*, 117–138, doi:10.1016/j.bcp.2016.09.018.

19. De La Fuente-Núñez, C.; Cardoso, M. H.; De Souza Cândido, E.; Franco, O. L.; Hancock, R. E. W. Synthetic antibiofilm peptides. *Biochim. Biophys. Acta - Biomembr.* **2016**, *1858*, 1061–1069, doi:10.1016/j.bbamem.2015.12.015.

20. Strempel, N.; Strehmel, J.; Overhage, J. Potential Application of Antimicrobial Peptides in the Treatment of Bacterial Biofilm Infections. *Curr. Pharm. Des.* **2015**, *21*, 67–84.

21. Tuson, H. H.; Weibel, D. B. Bacteria–surface interactions. *Soft Matter* **2013**, *9*, 4368, doi:10.1039/c3sm27705d.

22. Yu, Q.; Wu, Z.; Chen, H. Dual-function antibacterial surfaces for biomedical applications. *Acta Biomater.* **2015**, *16*, 1–13, doi:10.1016/j.actbio.2015.01.018.

23. Yan, S.; Song, L.; Luan, S.; Xin, Z.; Du, S.; Shi, H.; Yuan, S.; Yang, Y.; Yin, J. A hierarchical polymer brush coating with dual-function antibacterial capability. *Colloids Surfaces B Biointerfaces* **2017**, *150*, 250–260, doi:10.1016/j.colsurfb.2016.08.033.

24. Paris, J.-B.; Seyer, D.; Jouenne, T.; Thébault, P. Elaboration of antibacterial plastic surfaces by a combination of antiadhesive and biocidal coatings of natural products. *Colloids Surfaces B Biointerfaces* **2017**, *156*, 186–193, doi:10.1016/j.colsurfb.2017.05.025.

25. Gao, Q.; Yu, M.; Su, Y.; Xie, M.; Zhao, X.; Li, P.; Ma, P. X. Rationally designed dual functional block copolymers for bottlebrush-like coatings: In vitro and in vivo antimicrobial, antibiofilm, and antifouling properties. *Acta Biomater.* **2017**, *51*, 112–124, doi:10.1016/j.actbio.2017.01.061.

26. Yang, C.; Ding, X.; Ono, R. J.; Lee, H.; Hsu, L. Y.; Tong, Y. W.; Hedrick, J.; Yang, Y. Y. Brush-like polycarbonates containing dopamine, cations, and PEG providing a broad-spectrum, antibacterial, and antifouling surface via one-step coating. *Adv. Mater.* **2014**, *26*, 7346–7351, doi:10.1002/adma.201402059.

27. Su, Y.; Zhi, Z.; Gao, Q.; Xie, M.; Yu, M.; Lei, B.; Li, P.; Ma, P. X. Autoclaving-Derived Surface Coating with In Vitro and In Vivo Antimicrobial and Antibiofilm Efficacies. *Adv. Healthc. Mater.* **2017**, *6*, 1–15, doi:10.1002/adhm.201601173.

28. Zhi, Z.; Su, Y.; Xi, Y.; Tian, L.; Xu, M.; Wang, Q.; Padidan, S.; Li, P.; Huang, W. Dual-Functional Polyethylene Glycol-b-polyhexanide Surface Coating with in Vitro and in Vivo Antimicrobial and Antifouling Activities. *ACS Appl. Mater. Interfaces* **2017**, *9*, 10383–10397, doi:10.1021/acsami.6b12979.

29. Goodman, Stuart B.; Yao, Zhenyu; Keene, Michaell; Yang, F. The Future of Biologic Coatings for Orthopaedic Implants. *Biomaterials* **2013**, *34*, 3174–3183, doi:10.1016/j.biotechadv.2011.08.021.Secreted.

30. Raphel, J.; Holodniy, M.; Goodman, S. B.; Heilshorn, S. C. Multifunctional Coatings to Simultaneously Promote Osseointegration and Prevent Infection of Orthopaedic Implants. *Biomaterials* **2016**, *84*, 301–314, doi:10.1016/j.biomaterials.2016.01.016.

31. Goriainov, V.; Cook, R.; Latham, J. M.; Dunlop, D. G.; Oreffo, R. O. C. Bone and metal: an orthopaedic perspective on osseointegration of metals. *Acta Biomater.* **2014**, *10*, 4043–4057, doi:10.1016/j.actbio.2014.06.004.

32. Muszanska, A. K.; Rochford, E. T. J.; Gruszka, A.; Bastian, A. A.; Busscher, H. J.; Norde, W.; Van Der Mei, H. C.; Herrmann, A. Antiadhesive polymer brush coating functionalized with antimicrobial and RGD peptides to reduce biofilm formation and enhance tissue integration. *Biomacromolecules* **2014**, *15*, 2019–2026, doi:10.1021/bm500168s.

33. Bell, B. F.; Schuler, M.; Tosatti, S.; Textor, M.; Schwartz, Z.; Boyan, B. D. Osteoblast response to titanium surfaces functionalized with extracellular matrix peptide

biomimetics. *Clin. Oral Implants Res.* **2011**, *22*, 865–72, doi:10.1111/j.1600-0501.2010.02074.x.

34. Zhang, L.; Ning, C.; Zhou, T.; Liu, X.; Yeung, K. W. K.; Zhang, T.; Xu, Z.; Wang, X.; Wu, S.; Chu, P. K. Polymeric nanoarchitectures on Ti-based implants for antibacterial applications. *ACS Appl. Mater. Interfaces* **2014**, *6*, 17323–17345, doi:10.1021/am5045604.

35. Lin, W.; Junjian, C.; Chengzhi, C.; Lin, S.; Sa, L.; Li, R.; Yingjun, W. Multi-biofunctionalization of a titanium surface with a mixture of peptides to achieve excellent antimicrobial activity and biocompatibility. *J. Mater. Chem. B* **2015**, *3*, 30–33, doi:10.1039/C4TB01318B.

36. Hoyos-Nogués, M.; Velasco, F.; Ginebra, M.-P.; Manero, J. M.; Gil, F. J.; Mas-Moruno, C. Regenerating Bone via Multifunctional Coatings: The Blending of Cell Integration and Bacterial Inhibition Properties on the Surface of Biomaterials. *ACS Appl. Mater. Interfaces* **2017**, *9*, 21618–21630, doi:10.1021/acsami.7b03127.

37. Yüksel, E.; Karakeçili, A.; Demirtaş, T. T.; Gümüşderelioğlu, M. Preparation of bioactive and antimicrobial PLGA membranes by magainin II/EGF functionalization. *Int. J. Biol. Macromol.* **2016**, *86*, 162–168, doi:10.1016/j.ijbiomac.2016.01.061.

38. Godoy-Gallardo, M.; Guillem-Marti, J.; Sevilla, P.; Manero, J. M.; Gil, F. J.; Rodriguez, D. Anhydride-functional silane immobilized onto titanium surfaces induces osteoblast cell differentiation and reduces bacterial adhesion and biofilm formation. *Mater. Sci. Eng. C* **2016**, *59*, 524–532, doi:10.1016/j.msec.2015.10.051.

39. Costa, F.; Maia, S.; Gomes, J.; Gomes, P.; Martins, M. C. L. Characterization of hLF1-11 immobilization onto chitosan ultrathin films, and its effects on antimicrobial activity. *Acta Biomater.* **2014**, *10*, 3513–3521, doi:10.1016/j.actbio.2014.02.028.

40. Tanaka, Y.; Doi, H.; Iwasaki, Y.; Hiromoto, S.; Yoneyama, T.; Asami, K.; Imai, H.; Hanawa, T. Electrodeposition of amine-terminated poly(ethylene glycol) to titanium surface. *Mater. Sci. Eng. C* **2007**, *27*, 206–212, doi:10.1016/j.msec.2006.03.007.

41. Tanaka, Y.; Matin, K.; Gyo, M.; Okada, A.; Tsutsumi, Y.; Doi, H.; Nomura, N.; Tagami, J.; Hanawa, T. Effects of electrodeposited poly(ethylene glycol) on biofilm adherence to titanium. *J. Biomed. Mater. Res. - Part A* **2010**, *95*, 1105–1113, doi:10.1002/jbm.a.32932.

42. Buxadera-Palomero, J.; Calvo, C.; Torrent-Camarero, S.; Gil, F. J.; Mas-Moruno, C.; Canal, C.; Rodríguez, D. Biofunctional polyethylene glycol coatings on titanium: An in vitro-based comparison of functionalization methods. *Colloids Surfaces B Biointerfaces* **2017**, *152*, 367–375, doi:10.1016/j.colsurfb.2017.01.042.

43. Mas-Moruno, C.; Fraioli, R.; Rechenmacher, F.; Neubauer, S.; Kapp, T. G.; Kessler, H. αvβ3- or α5β1-Integrin-Selective Peptidomimetics for Surface Coating. *Angew. Chemie - Int. Ed.* **2016**, *55*, 7048–7067, doi:10.1002/anie.201509782.

44. Bellis, S. L. Advantages of RGD peptides for directing cell association with biomaterials. *Biomaterials* **2011**, *32*, 4205–4210, doi:10.1016/j.biomaterials.2011.02.029.

45. Hoyos-Nogués, M.; Brosel-Oliu, S.; Abramova, N.; Muñoz, F. X.; Bratov, A.; Mas-Moruno, C.; Gil, F. J. Impedimetric antimicrobial peptide-based sensor for the early detection of periodontopathogenic bacteria. *Biosens. Bioelectron.* **2016**, *86*, 377–385, doi:10.1016/j.bios.2016.06.066.

46. Mas-Moruno, C.; Fraioli, R.; Albericio, F.; Manero, J. M.; Gil, F. J. Novel peptide-based platform for the dual presentation of biologically active peptide motifs on biomaterials. *ACS Appl. Mater. Interfaces* **2014**, *6*, 6525–6536, doi:10.1021/am5001213.

47. Buxadera-palomero, J.; Carrasco, P.; Albó, K.; Gil, F. J.; Rodríguez, D. *Polyethylene glycol pulsed electrodeposition for the design of antifouling coatings on titanium*;

48. Fraioli, R.; Dashnyam, K.; Kim, J.-H.; Perez, R. A.; Kim, H.-W.; Gil, J.; Ginebra, M.-P.; Manero, J. M.; Mas-Moruno, C. Surface guidance of stem cell behavior: Chemically tailored co-presentation of integrin-binding peptides stimulates osteogenic differentiation in vitro and bone formation in vivo. *Acta Biomater.* **2016**, *43*, 269–281, doi:10.1016/j.actbio.2016.07.049.

49. Fraioli, R.; Rechenmacher, F.; Neubauer, S.; Manero, J. M.; Gil, J.; Kessler, H.; Mas-Moruno, C. Mimicking bone extracellular matrix: Integrin-binding peptidomimetics enhance osteoblast-like cells adhesion, proliferation, and differentiation on titanium. *Colloids Surfaces B Biointerfaces* **2015**, *128*, 191–200, doi:10.1016/j.colsurfb.2014.12.057.

50. Le Guéhennec, L.; Soueidan, A.; Layrolle, P.; Amouriq, Y. Surface treatments of titanium dental implants for rapid osseointegration. *Dent. Mater.* **2007**, *23*, 844–54, doi:10.1016/j.dental.2006.06.025.

51. Neoh, K. G.; Hu, X.; Zheng, D.; Kang, E. T. Balancing osteoblast functions and bacterial adhesion on functionalized titanium surfaces. *Biomaterials* **2012**, *33*, 2813–2822, doi:10.1016/j.biomaterials.2012.01.018.

52. Bollen, C. M.; Papaioanno, W.; Van Eldere, J.; Schepers, E.; Quirynen, M.; van Steenberghe, D. The influence of abutment surface roughness on plaque accumulation and peri-implant mucositis. *Clin. Oral Implants Res.* **1996**, *7*, 201–211, doi:10.1034/j.1600-0501.1996.070302.x.

53. Deligianni, D. D.; Katsala, N.; Ladas, S.; Sotiropoulou, D.; Amedee, J.; Missirlis, Y. F. Effect of surface roughness of the titanium alloy Ti-6Al-4V on human bone marrow cell response and on protein adsorption. *Biomaterials* **2001**, *22*, 1241–1251, doi:10.1016/S0142-9612(00)00274-X.

54. Aronsson, B. O.; Lausmaa, J.; Kasemo, B. Glow discharge plasma treatment for surface cleaning and modification of metallic biomaterials. *J. Biomed. Mater. Res.* **1997**, *35*, 49–73, doi:10.1002/(SICI)1097-4636(199704)35:1<49::AID-JBM6>3.0.CO;2-M.

55. Nisol, B.; Oldenhove, G.; Preyat, N.; Monteyne, D.; Moser, M.; Perez-Morga, D.; Reniers, F. Atmospheric plasma synthesized PEG coatings: Non-fouling biomaterials showing protein and cell repulsion. *Surf. Coatings Technol.* **2014**, *252*, 126–133, doi:10.1016/j.surfcoat.2014.04.056.

56. Snavely, D. L.; Dubsky, J. Near-IR spectra of polyethylene, polyethylene glycol, and polyvinylethyl ether. *J. Polym. Sci. Part A Polym. Chem.* **1996**, *34*, 2575–2579, doi:10.1002/(SICI)1099-0518(19960930)34:13<2575::AID-POLA3>3.0.CO;2-R.

57. Fabian, H.; Mäntele, W. Infrared Spectroscopy of Proteins - Handbook of Vibrational Spectroscopy. **2002**, 1–27, doi:10.1002/0470027320.s8201.

58. Ploux, L.; Ponche, A.; Anselme, K. Bacteria/material interfaces: role of the material and cell wall properties. *J. Adhes. Sci. Technol.* **2010**, *24*, 2165–2201, doi:10.1163/016942410X511079.

59. Molena, E.; Credi, C.; De Marco, C.; Levi, M.; Turri, S.; Simeone, G. Protein antifouling and fouling-release in perfluoropolyether surfaces. *Appl. Surf. Sci.* **2014**, *309*, 160–167, doi:10.1016/j.apsusc.2014.04.211.

60. Pegueroles, M.; Tonda-Turo, C.; Planell, J. A.; Gil, F. J.; Aparicio, C. Adsorption of fibronectin, fibrinogen, and albumin on TiO2: Time-Resolved Kinetics, structural changes, and competition study. *Biointerphases* **2012**, *7*, 1–13, doi:10.1007/s13758-012-0048-4.

61. Subbiahdoss, G.; Pidhatika, B.; Coullerez, G.; Charnley, M.; Kuijer, R.; van der Mei, H.; Textor, M.; Busscher, H. Bacterial biofilm formation versus mammalian cell growth on titanium-based mono- and bi-functional coating. *Eur. Cells Mater.* **2010**, *19*, 205–213, doi:10.22203/eCM.v019a20.

62. Arciola, C. R.; Bustanji, Y.; Conti, M.; Campoccia, D.; Baldassarri, L.; Samorì, B.; Montanaro, L. Staphylococcus epidermidis-fibronectin binding and its inhibition by heparin. *Biomaterials* **2003**, *24*, 3013–3019, doi:10.1016/S0142-9612(03)00133-9.

63. Kapp, T. G.; Rechenmacher, F.; Neubauer, S.; Maltsev, O. V.; Cavalcanti-Adam, E. A.; Zarka, R.; Reuning, U.; Notni, J.; Wester, H.-J.; Mas-Moruno, C.; Spatz, J.; Geiger, B.; Kessler, H. A Comprehensive Evaluation of the Activity and Selectivity Profile of Ligands for RGD-binding Integrins. *Sci. Rep.* **2017**, *7*, 39805, doi:10.1038/srep39805.

64. Mas-Moruno, C.; Dorfner, P. M.; Manzenrieder, F.; Neubauer, S.; Reuning, U.; Burgkart, R.; Kessler, H. Behavior of primary human osteoblasts on trimmed and sandblasted Ti6Al4V surfaces functionalized with integrin avb3-selective cyclic RGD

peptides. *J. Biomed. Mater. Res. - Part A* **2013**, *101 A*, 87–97, doi:10.1002/jbm.a.34303.

65. Zhao, B.; Van Der Mei, H. C.; Subbiahdoss, G.; De Vries, J.; Rustema-Abbing, M.; Kuijer, R.; Busscher, H. J.; Ren, Y. Soft tissue integration versus early biofilm formation on different dental implant materials. *Dent. Mater.* **2014**, *30*, 716–727, doi:10.1016/j.dental.2014.04.001.

66. Peng, L.; Chang, L.; Liu, X.; Lin, J.; Liu, H.; Han, B.; Wang, S. Antibacterial Property of a Polyethylene Glycol-Grafted Dental Material. *ACS Appl. Mater. Interfaces* **2017**, *9*, 17688–17692, doi:10.1021/acsami.7b05284.

67. Godoy-Gallardo, M.; Mas-Moruno, C.; Yu, K.; Manero, J. M.; Gil, F. J.; Kizhakkedathu, J. N.; Rodriguez, D. Antibacterial Properties of hLf1–11 Peptide onto Titanium Surfaces: A Comparison Study Between Silanization and Surface Initiated Polymerization. *Biomacromolecules* **2015**, *16*, 483–496, doi:10.1021/bm501528x.

68. Nagano-Takebe, F.; Miyakawa, H.; Nakazawa, F.; Endo, K. Inhibition of initial bacterial adhesion to titanium by lactoferrin. *Biointerphases* **2014**, *26*, 39, doi:10.1116/1.4867415.

69. Ferraris, S.; Spriano, S. Antibacterial titanium surfaces for medical implants. *Mater. Sci. Eng. C* **2015**, *61*, 965–978, doi:10.1016/j.msec.2015.12.062.